

## High-Energy Elastic Scattering of $\pi^\pm$ , $K^-$ , and $\bar{p}$ on Hydrogen at c.m. Angles from $22^\circ$ to $180^\circ$ \*

D. P. OWEN, F. C. PETERSON,<sup>†</sup> J. OREAR, A. L. READ,<sup>‡</sup> D. G. RYAN,<sup>§</sup> AND D. H. WHITE  
*Laboratory of Nuclear Studies, Cornell University, Ithaca, New York 14850*

AND

A. ASHMORE,<sup>||</sup> C. J. S. DAMERELL,<sup>\*\*</sup> W. R. FRISKEN,<sup>††</sup> AND R. RUBINSTEIN  
*Brookhaven National Laboratory, Upton, New York 11973*

(Received 31 January 1969)

Elastic  $\pi^\pm$ - $p$ ,  $K^-$ - $p$ , and  $\bar{p}$ - $p$  scattering cross sections have been measured using three different experimental arrangements covering the c.m. angular regions  $\sim 20^\circ$ - $120^\circ$ ,  $\sim 135^\circ$ - $169^\circ$ , and  $\sim 165^\circ$ - $180^\circ$  at incident momenta from 6 to 17 GeV/c. In the region  $130^\circ$ - $180^\circ$ , only  $\pi^\pm$ - $p$  scattering was measured. In the angular region near  $180^\circ$ , the energy dependences and shapes of the  $\pi$ - $p$  backward peaks were determined up to crossed-momentum transfers of  $u \sim -2$  (GeV/c)<sup>2</sup>. At all energies, the  $\pi^+$ - $p$  backward peak had a sharp dip at  $u = -0.13$  (GeV/c)<sup>2</sup>, with no similar effect in the  $\pi^-$ - $p$  case. Nearly complete angular distributions of  $\pi^-$ - $p$  elastic scattering from  $20^\circ$  to  $180^\circ$  have been obtained at 6 and 10 GeV/c. These results at 6 and 10 GeV/c as well as at 8 GeV/c reveal a sharp dip in  $\pi^-$ - $p$  scattering at  $t = -3$  (GeV/c)<sup>2</sup>. Several structures in the form of dips or shoulders were seen in the  $\bar{p}$ - $p$  angular distributions also, with less pronounced structure observed in  $K^-$ - $p$  scattering. At fixed momentum transfer, all cross sections when expressed as  $d\sigma/dt$  appear to be decreasing with increasing energy.

### I. INTRODUCTION

RECENT work has established the existence of rather sharp and striking backward peaks in  $\pi$ - $p$  elastic scattering.<sup>1,2</sup> It now seems reasonably well established that whenever the exchange of a known baryon at low-momentum transfer would predict a backward peak, then, and only then, is such a peak seen in the angular distribution at high energies (energies above the region of direct channel resonance contributions).<sup>2</sup> The purpose of the present experiment was to measure with improved accuracy the  $\pi^+$ - $p$  and  $\pi^-$ - $p$  backward peaks at higher energies and higher crossed-momentum transfers than before. The earlier indication<sup>1,3</sup> of a dip in the  $\pi^+$ - $p$  backward peak at  $u = -0.13$  (GeV/c)<sup>2</sup> has been confirmed and appears to become deeper with increasing energy. The lack of such a dip in the  $\pi^-$ - $p$  backward peak has been presented as evidence in favor of Reggeized baryon exchange<sup>1,2,4</sup> and our results have been interpreted as supporting this view.<sup>4</sup>

\* Research supported by a National Science Foundation research grant and by the U. S. Atomic Energy Commission.

<sup>†</sup> Present address: Department of Physics, Iowa State University, Ames, Ia.

<sup>‡</sup> Present address: National Accelerator Laboratory, Batavia, Ill.

<sup>§</sup> Present address: Department of Physics, McGill University, Montreal, Quebec, Canada.

<sup>||</sup> Permanent address: Queen Mary College, London, England.

\*\* Rutherford High Energy Laboratory Fellow.

<sup>††</sup> Present address: Department of Physics, Case Western Reserve University, Cleveland, Ohio.

<sup>1</sup> J. Orear, R. Rubinstein, D. B. Scarf, D. H. White, A. D. Krisch, W. R. Frisken, A. L. Read, and H. Ruderman, *Phys. Rev.* **152**, 1162 (1966). This paper contains references to earlier work.

<sup>2</sup> For a more recent summary of backward peaks, see the review by M. Derrick, in CERN Report No. 68-7, Vol. I, p. 111 (unpublished).

<sup>3</sup> H. Brody, R. Lanza, R. Marshall, J. Niederer, W. Selove, M. Shochet, and R. Van Berg, *Phys. Rev. Letters* **16**, 828 (1966); **16**, 968 (1966).

<sup>4</sup> V. Barger and D. Cline, *Phys. Rev. Letters* **21**, 392 (1968).

We have complemented the  $\pi^-$ - $p$  backward-peak measurements at 6, 10, and 14 GeV/c, with measurements using "forward" geometries which covered the range  $22^\circ < \theta_{c.m.} < 120^\circ$ ; up to now, there has been little information on large-angle  $\pi$ - $p$  elastic scattering at high energies. When combined with the smaller-angle results,<sup>5</sup> our new results give a reasonable idea of the complete  $\pi^-$ - $p$  angular distribution at 6 and 10 GeV/c. In addition, elastic  $\bar{p}$ - $p$  and  $K^-$ - $p$  distributions were simultaneously obtained up to momentum transfers of  $t \sim -6$  (GeV/c)<sup>2</sup>.

Some of the data presented in this paper have been reported earlier in preliminary form.<sup>6-9</sup> This paper presents the completed analysis of all the data and a more detailed discussion of the experimental technique and theoretical implications. Additional information on the experimental method and data analysis is contained in the Ph.D. theses of two of the coauthors.<sup>10,11</sup>

### II. EXPERIMENTAL METHOD

The  $4.5^\circ$  momentum-analyzed secondary beam<sup>12</sup> of the Brookhaven AGS was scattered by a 24-in. liquid-hydrogen target. Both the scattered particle and recoil proton were momentum-analyzed and detected in scintillation-counter telescopes, up to 12 for the pion

<sup>5</sup> K. J. Foley, S. J. Lindenbaum, W. A. Love, S. Ozaki, J. J. Russell, and L. C. L. Yuan, *Phys. Rev. Letters* **10**, 376 (1963); **11**, 425 (1963); **11**, 503 (1963).

<sup>6</sup> A. Ashmore, C. J. S. Damerell, W. R. Frisken, R. Rubinstein, J. Orear, D. P. Owen, F. C. Peterson, A. L. Read, D. G. Ryan, and D. H. White, *Phys. Rev. Letters* **19**, 460 (1967).

<sup>7</sup> A. Ashmore *et al.*, *Phys. Rev. Letters* **21**, 387 (1968).

<sup>8</sup> J. Orear *et al.*, *Phys. Rev. Letters* **21**, 389 (1968).

<sup>9</sup> J. Orear *et al.*, *Phys. Letters* **28B**, 61 (1968).

<sup>10</sup> F. C. Peterson, Cornell University thesis, 1968 (unpublished).

<sup>11</sup> D. P. Owen, Cornell University thesis, 1969 (unpublished).

<sup>12</sup> A. L. Read and R. Rubinstein, Brookhaven National Laboratory Report No. BNL-9213 (unpublished).

and up to six for the proton. A triple coincidence between the incident beam telescope, any pion telescope, and any proton telescope was used to trigger optical spark chambers which recorded tracks of the scattered particles. Beam pions, kaons, protons, and antiprotons were identified by appropriate pulses from a threshold gas Čerenkov counter<sup>13</sup> detecting pions and two differential gas Čerenkov counters<sup>14</sup> tuned to the kaon and proton masses, respectively. Electron and muon contamination of the pions was also measured. In order to cover c.m. angles from  $20^\circ$  to  $180^\circ$ , three different experimental arrangements were used which we shall call forward geometry, intermediate geometry, and back geometry.

### A. Forward Geometry

This was used for negative beam particles of 5.9, 7.9, 9.8, and 13.6 GeV/c. The experimental arrangement is shown in Fig. 1. Both the scattered and recoil particles were momentum-analyzed by the magnet  $M$  of aperture 10 ft wide by 2 ft high. The effective field was about 15 kG over a length of 3 ft. At 9.8 GeV/c, the magnet aperture subtended an angular range  $71^\circ < \theta_{c.m.} < 122^\circ$ , as shown in Fig. 1. In order to cover the angular region  $23^\circ < \theta_{c.m.} < 72^\circ$ , the beam (and hydrogen target) was displaced by  $\sim 1$  ft, using a bending magnet in the beam upstream of the target. The two positions are designated forward geometry 1 ( $23^\circ < \theta_{c.m.} < 72^\circ$ ) and forward geometry 2 ( $71^\circ < \theta_{c.m.} < 122^\circ$ ).

In Fig. 1 the positions of scintillation counters in the six pion telescopes are shown as  $\pi_1, \pi_2, \pi_3$ . Adjacent  $\pi_3$  counters were touching so that the full angular region

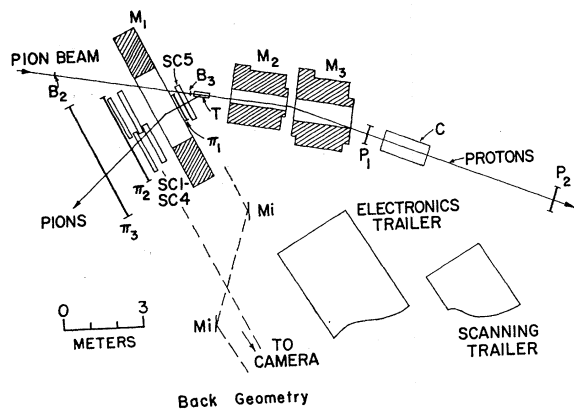


FIG. 1. Forward geometry. SC<sub>1</sub>, SC<sub>2</sub>, SC<sub>3</sub>, and SC<sub>4</sub> are optical spark chambers;  $\pi_1, \pi_2, \pi_3, P_1, P_2$ , and  $P_3$  represent banks of scintillation counters; M is the large-aperture magnet; B<sub>2</sub> and B<sub>3</sub> are beam scintillation counters; T is the liquid-hydrogen target. Not shown are a counter B<sub>1</sub> and one threshold and two differential gas Čerenkov counters in the incident beam. Also not shown are several anticoincidence counters.

<sup>13</sup> R. Rubinstein, Brookhaven National Laboratory Report No. BNL-9466 (unpublished).

<sup>14</sup> T. F. Kycia and E. W. Jenkins, *Nuclear Electronics* (International Atomic Energy Agency, Vienna, 1962), Vol. I, p. 63.

was covered; the  $\pi_1$  and  $\pi_2$  scintillators were large enough to detect all elastically scattered pions that reached the appropriate  $\pi_3$ . A similar arrangement was used for the six proton telescope scintillators at positions  $P_1, P_2$ , and  $P_3$ . A triple coincidence between any pion telescope, any proton telescope, and the beam telescope was used to trigger the spark chambers SC1–SC4. The trigger pulse could be vetoed by a number of anti-coincidence counters which are not shown; these were placed to reject “beam” particles outside the beam telescope, noninteracting beam, particles scattered at angles not covered by the  $\pi$  and  $P$  telescopes, and to protect the  $\pi$  and  $P$  scintillators from interactions in the B<sub>3</sub> counter.

At 9.8 GeV/c the beam intensity, defined by the  $1\frac{1}{2}$ -in. vertical  $\times 1\frac{3}{4}$ -in. horizontal counter B<sub>3</sub>, was  $\sim 5 \times 10^6$  particles (93%  $\pi^-$ , 3.5%  $\mu^-$ , 2%  $K^-$ , 1%  $\bar{p}$ , 0.5%  $e^-$ ) per AGS pulse, and gave  $\sim 1$  trigger per 3 AGS pulses. Elastic events were between 0.3 and 70% of the total number of triggers, depending on angle and energy. The lowest percentage of elastic events was obtained in forward geometry 2 at 9.8 GeV/c, where the cross sections were  $\sim 10^{-7}$  of the forward cross section. As will be seen in Sec. II E, the spark chambers provided adequate spatial resolution to separate the elastic scattering events from other processes.

### B. Intermediate Geometry

This geometry was used for positive pions at 5.9, 9.9, and 13.7 GeV/c and for negative pions at 5.9 and 9.9 GeV/c. The experimental arrangement is shown in Fig. 2. The large-aperture magnet M<sub>1</sub> was used to momentum-analyze pions only, and the forward-going recoil protons were momentum-analyzed by magnet M<sub>2</sub>, with aperture 30 in. wide by 12 in. high by 72 in. long. At 9.9 GeV/c the angles subtended by both magnets were such that the angular range  $135^\circ < \theta_{c.m.} < 169^\circ$  was covered. The  $\pi_3$  counter for each pion telescope was

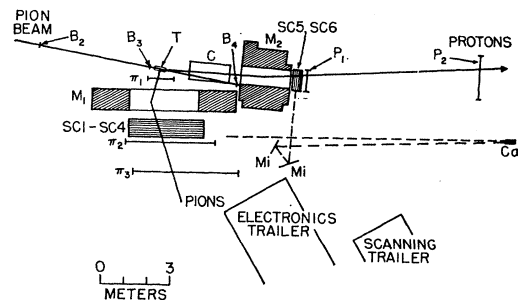


FIG. 2. Intermediate geometry. Scattered pions pass through magnet M<sub>1</sub> and spark chambers SC1–SC4. Forward recoil protons pass through threshold gas Čerenkov counter C, magnet M<sub>2</sub>, and spark chambers SC5 and SC6. The symbols  $\pi_1, \pi_2, \pi_3, P_1$ , and  $P_2$  stand for banks of scintillation counters. The liquid-hydrogen target is T, Mi are mirrors, and Ca is the camera. B<sub>2</sub>–B<sub>4</sub> are beam counters. Not shown are counter B<sub>1</sub> and a threshold Čerenkov counter in the beam.

18 in. horizontal  $\times$  36 in. vertical, consisting of signals fanned in from two 18 $\times$ 18 in. scintillators. Hence, the pion solid angle was defined by a 15 $\times$ 3 ft "wall" of scintillator. A threshold gas Čerenkov counter C (Freon at 1 atm) was used to veto forward-scattered pions.

Trigger rates were  $\sim 1$  every 5 pulses for a typical beam intensity of  $\sim 4 \times 10^6$  pions/pulse. The elastic events ranged from 20 to 1% of the triggers for beam momenta of 5.9 and 13.7 GeV/ $c$ , respectively.

### C. Back Geometry

This geometry was used for positive pions of 5.9, 9.9, 13.7, and 17.1 GeV/ $c$  and for negative pions of 5.9, 9.9, 13.7 and 16.3 GeV/ $c$ . As shown in Fig. 3, the experimental arrangement was similar to that of the intermediate geometry, except that the large aperture magnet was moved to subtend angles to  $180^\circ$ , with the consequence that the incident beam also passed through this magnet. The angular region covered was  $163^\circ < \theta_{e.m.} < 180^\circ$ , which overlapped somewhat with the intermediate geometry. In order to increase the momentum resolution on the protons at all momenta except 5.9 GeV/ $c$ , two magnets  $M_2$  and  $M_3$  were used to give almost four times the deflection used in the intermediate geometry. Threshold gas Čerenkov counter C was again used to veto forward pions. There were 11 pion telescopes with each  $\pi_3$  counter subtending 18 in. horizontal by 36 in. vertical. The position and angle of the back-scattered pion were measured by the spark chambers SC5 before magnetic analysis and SC1-SC4 after deflection by  $M_1$ . The overdetermination provided by SC5 and the proton telescope information was sufficient to eliminate inelastic background, as discussed in Sec. II G. Typical intensities were  $5 \times 10^5$  incident particles/pulse giving  $10^{-1}$ – $10^{-2}$  triggers/pulse. The fraction of elastic events varied from 33 to 2% of the triggers, depending on the beam momentum.

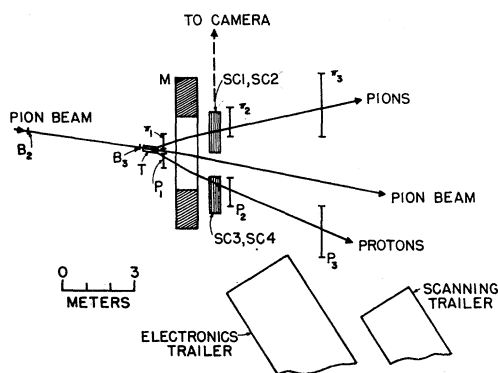


FIG. 3. Back geometry. Back-scattered pions pass through magnet  $M_1$  and spark chambers SC1-SC4. Forward recoil protons pass through magnets  $M_2$  and  $M_3$ . The symbols  $\pi_1$ ,  $\pi_2$ ,  $\pi_3$ ,  $P_1$ , and  $P_2$  stand for banks of scintillation counters.  $B_2$  and  $B_3$  are beam counters, T is the liquid-hydrogen target, C is a threshold gas Čerenkov counter, and  $M_i$  are mirrors.

### D. Electronics System

This can be divided into fast and slow logic systems.

The fast logic system consisted of commercially available logic units<sup>15</sup> which standardized pulses from the counters and developed the appropriate coincidence combinations to generate the master trigger pulse. Detailed logic diagrams are given in Ref. 10. Any pion telescope in combination with any proton telescope in coincidence with the beam telescope gave a master trigger. However, provision was made for triggering on any selected pion-proton combinations if the trigger rates using all combinations had been too great, but this was rarely used. The information as to which pion-proton telescope combination and which beam Čerenkov counter corresponded to each trigger was recorded both on magnetic tape and in the memory of a 2-dimensional pulse-height analyzer. In forward geometry 1, because of the very rapid decrease of cross section with angle, most of the triggers came from the smallest angle pion telescope. The fast logic was designed so that, after an appropriate amount of data-taking, the smaller angle  $\pi$ - $p$  triggers could be switched off without losing the smaller angle  $K^-$ - $p$  and  $\bar{p}$ - $p$  triggers.

The slow logic<sup>11</sup> consisted mainly of custom-built electronics to control the camera and spark chambers and to interface the fast logic to a tape recorder, the pulse-height analyzer, and film-recorded information using nixies and flash tubes alongside the spark chambers. Information stored in one or more of the three modes was frame number, proton telescope number, pion telescope number, Čerenkov counter number, total incident beam, and the time difference between  $\pi_3$  and  $P_3$  counter pulses. This time difference was measured to determine the number of accidental coincidences; it was found that the accidental rate was negligible for all geometries. Individual beam and telescope rates were recorded on fast scalars which were printed out at the end of each run. Although the information in the pulse-height analyzer display was redundant, it was particularly useful in the early stages of the experiment in estimating and optimizing the percentage of good triggers; it and the fast scalars were also useful for monitoring the components of the system for possible failures.

### E. Spark Chambers

The large spark chambers were thin foil (1 mil aluminum) of 62 $\times$ 28 in. sensitive region. Two such chambers of four gaps each side by side covered the 120 $\times$ 24 in. aperture of the large aperture magnet. Another pair of chambers with six gaps each was placed 18 in. behind the first pair in order to obtain adequate angular resolution of tracks. Each particle thus traversed a total of 10 gaps of  $\frac{3}{8}$  in. per gap. Chambers SC5 and SC6 of Fig. 2 were constructed similarly and

<sup>15</sup> Chronetics, Inc., Mt. Vernon, N. Y.

had an active area of  $36 \times 15$  in. The time delay between the passage of a particle through the chambers and the actual firing was about 500 nsec, and the clearing fields were adjusted to give essentially 100% efficiency for these tracks and progressively less efficiency for older tracks. Chamber SC5 in the back geometry (Fig. 3) was the only one found to be not 100% efficient; its efficiency was usually  $\sim 90\%$  but was occasionally as low as 70% due to the high flux of the incident beam passing through the sensitive region of the chamber and causing some spark robbing. For each run the inefficiency of SC5 was determined by observing how often "good" tracks would appear in SC1-SC4 but not in SC5. This correction, which amounted to as much as 30%, is discussed further in Sec. II H.

The chambers were each pulsed by a spark gap<sup>16</sup> triggered by a spark amplifier<sup>16</sup> driven directly from the fast logic.

Each chamber was photographed in  $90^\circ$  stereo, one view directly and the other by means of a  $45^\circ$  mirror mounted above the chamber. In order to avoid the use of field lenses, the camera was placed 50 ft from the chambers, with aperture  $f/8$  and demagnification of  $100\times$ . The spark measuring accuracy obtained was typically  $\pm 0.05$  in. in real space, which corresponded to an accuracy in track angle of 1-2 mrad. Since this was comparable to the angular spread of the incident beam, there was no need for a more accurate system. Increased accuracy could only have been obtained by placing spark chambers in the incident beam to record the direction of each incoming track. However, this would have required a considerable reduction in beam intensity, with the result that many of the cross sections measured here would have been unattainable.

### F. Analysis

The method of analysis was the same for the forward and intermediate geometries. From the measured angle of the pion track, the analysis program assigned a pion momentum corresponding to an elastic event. The pion trajectory was then traced back through the large aperture magnet and the closest distance of approach to the hydrogen target determined. At the position of closest distance of approach an elastic scattering was again assumed with the beam pion exactly parallel to the beam direction; this then determined the recoil proton angle and momentum. The program then calculated the proton trajectory through its analyzing magnet and predicted the horizontal and vertical coordinates of the proton track in the proton spark chambers and the horizontal and vertical angles of the track. These four predictions were then compared with the four measured quantities. A histogram of the predicted minus the measured quantity showed an elastic peak sitting on a slowly varying background; Fig. 4 shows

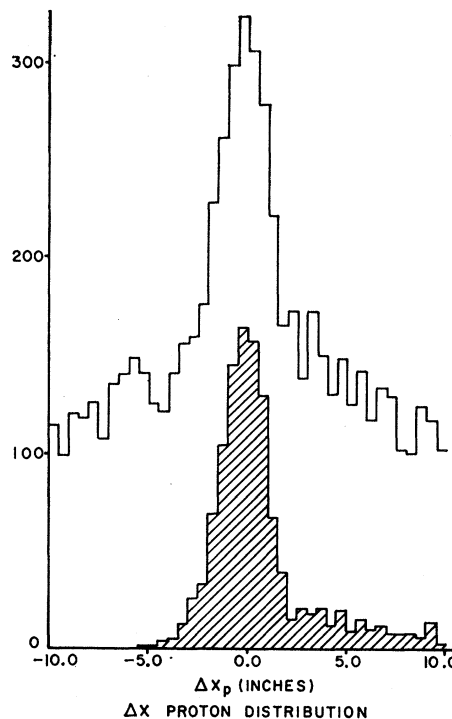


FIG. 4. Histogram of 9.9-GeV/ $c$   $\pi^-p$  events in intermediate geometry, showing deviation from expected position in proton spark chambers.  $\Delta x_p$  is the predicted-minus-the-measured horizontal coordinate in the proton spark chambers. The shaded histogram is the same except that events have been rejected which fall outside the target cuts or which fall outside the elastic peaks in the three other plots described in the text.

such a histogram for the intermediate geometry. In the shaded histogram of Fig. 4 events having a closest distance of approach to the target greater than 2 in. or which appeared well outside the elastic peak in one of the three other histograms were rejected. We see that very few inelastic events manage to survive these cuts.

In the back geometry the proton track was not measured by spark chambers. In this case the necessary overdetermination of the elastic scattering was given by chamber SC5, shown in Fig. 3. Using the measured track angle in SC1-SC4, the program assigned a pion momentum assuming elastic kinematics and traced the trajectory back to the point of closest approach to the hydrogen target. The program also predicted where the corresponding recoil proton would hit the  $P_2$  scintillators and predicted the horizontal and vertical positions in SC5. A typical histogram of predicted-minus-measured horizontal position in SC5 is shown as the upper histogram of Fig. 5. The lower histogram is obtained after rejecting those events whose predicted minus measured vertical position in SC5 is greater than  $\pm 1.3$  in. and those whose corresponding recoil proton would have passed through a proton telescope other than that which gave the trigger (obtained from the magnetic tape record); allowance was made for beam

<sup>16</sup> Science Accessories Corp., Southport, Conn.

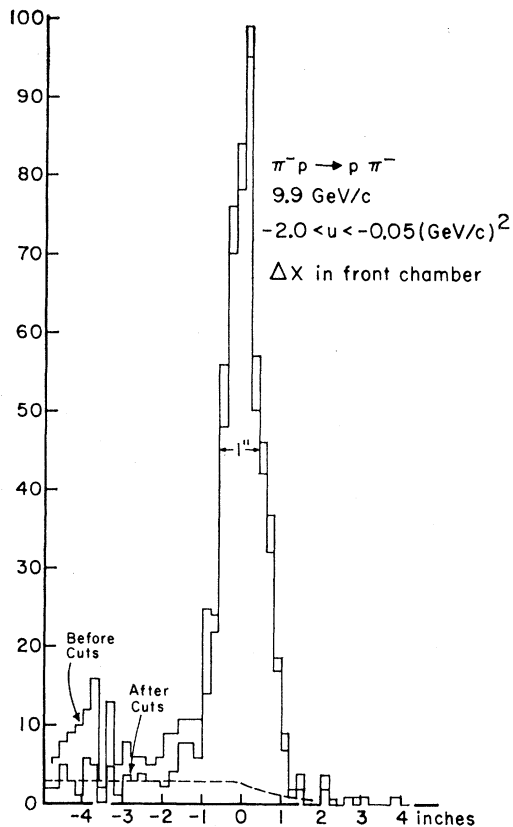


FIG. 5. Histogram of 9.9-GeV/c  $\pi^-p$  events in back geometry showing deviation from expected horizontal position in SC5 (the front spark chamber). The lower curve is obtained after making cuts on vertical position and proton counter telescope.

divergence and multiple scattering of the predicted recoil proton.

The analysis program was quite economical of computer time since an iterative procedure was not used in obtaining a best fit. In addition, the simplest parameterization of the magnetic fields consistent with the over-all experimental accuracy was used in all calculations.

Most of the results in this paper are based on hand measurements of the film using commercially available digitized measuring machines.<sup>17</sup> However, preliminary results for the back geometry<sup>6</sup> were obtained by running most of the back geometry film through the Brookhaven National Laboratory (BNL) Physics Department flying spot digitizer.<sup>18</sup> This system was quite useful in the early stages of the experiment since an "off-line" turnaround of 2 or 3 days could be obtained and used to improve the experimental design or running conditions. However, it was found that this system tended to reject 20 to 50% of the pictures (which then had to be hand measured). Hand measuring was both more efficient

(~98% compared to ~70%) and somewhat more accurate than the flying spot digitizer, and also the latter was unable to handle the multitrack condition of SC5. The preliminary back geometry results of Ref. 6 were based mainly on machine measuring of SC1-SC4 and hand measuring of a partial sample of the horizontal view of SC5. The results given in this paper are based on all the SC5 data in both views and supersede those of Ref. 6.

## G. Inelastic Background

### 1. Back Geometry

In the back geometry the correction for inelastic events was made using the information from SC5, as illustrated in Fig. 5. We use the fact that inelastic pions at a given lab angle have lower momentum than elastic. Thus inelastic events give negative values for  $\Delta x$  (the predicted-minus-measured horizontal position) in SC5, where the positive direction for the  $x$  axis is away from the trailers (see Fig. 3). The fact that the distribution of  $\Delta x$  shown in Fig. 5 has no tail in the positive region of  $\Delta x$  confirms that the negative tail is due to inelastic pions. The inelastic tails obtained were all rather flat over the entire region of negative  $\Delta x$ ; the procedure was to extrapolate these flat tails into the elastic peak and to assume that the inelastic background level under the elastic peak was  $(75 \pm 38)\%$  of the level outside the peak at negative  $\Delta x$ . This assumption was confirmed (although not with high statistical accuracy) by studying those events whose protons passed through a  $P_2$  counter that could not correspond to an elastic event. Where statistics were poor, fluctuations in background level over nearby scattering angles were smoothed out.

For negative pions, the inelastic subtraction was always less than 10% at 5.9 and 9.9 GeV/c, but became as high as 20% in the region  $169^\circ < \theta_{e.m.} < 176^\circ$  for 13.7 and 16.3 GeV/c. For positive pions in the region of the dip [ $u \approx -0.15$  (GeV/c)<sup>2</sup>], about  $\frac{1}{3}$  of the events under the elastic peak were found to be inelastic, but for  $\theta_{e.m.}$  near  $180^\circ$ , this correction was only a few percent.

The backward inelastic scattering process  $\pi^\pm + p \rightarrow \Delta^\pm + \pi^\pm$  could also give a peak in the  $\Delta x$  distribution of Fig. 5, and for 9.9 GeV/c and higher such a peak would somewhat overlap the elastic peak. However, less than 10% of the  $\Delta^+$  decays could simulate an elastically scattered proton within the resolution of our proton telescopes, and at least in the region 3-6 GeV/c the cross section for backward  $\pi^- + p \rightarrow \Delta^\pm + \pi^\mp$  is less than 10% of backward elastic.<sup>19</sup> We thus conclude that such a contribution to our results is negligible.

### 2. Intermediate and Forward Geometries

In these geometries spark chambers were used for the scattered protons as well as for the pions, with the

<sup>19</sup> R. Anthony, C. T. Coffin, E. Meanley, J. Rice, N. Stanton, and K. Terwilliger, Phys. Rev. Letters **21**, 1605 (1968); and paper submitted to the 1968 Vienna Conference on High Energy Physics (unpublished).

<sup>17</sup> The MicroMetric Corp., Berkeley, Calif.

<sup>18</sup> W. F. Baker, Brookhaven National Laboratory Report No. BNL-7404. (unpublished).

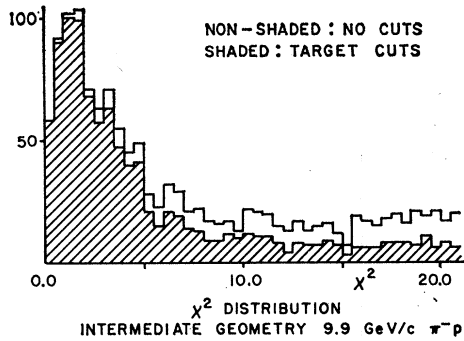


FIG. 6.  $\chi^2$  distribution of the nonshaded events in Fig. 4. The shaded distribution is obtained by making target cuts only.

result that an elastic event was more over determined than in the back geometry. An elastic peak was seen in each distribution of  $\Delta x$ ,  $\Delta y$ ,  $\Delta x'$ , and  $\Delta y'$ , where  $\Delta x$  and  $\Delta y$  are the predicted-minus-measured horizontal and vertical positions in the proton spark chamber and  $\Delta x'$  and  $\Delta y'$  are the corresponding quantities for the horizontal and vertical angles. A  $\chi^2$  value for each event was calculated using the four variables  $\Delta x$ ,  $\Delta y$ ,  $\Delta x'$  and  $\Delta y'$ , all normalized to their measured central value and weighted according to their experimental width. A typical  $\chi^2$  distribution is shown in Fig. 6. Although four degrees of freedom were used, they are not completely independent, since, for example, the vertical position and angle of a track were coupled. It was found that the  $\chi^2$  distributions were flat outside the peak, which would correspond to an effective two degrees of freedom. Monte Carlo investigations gave  $(75 \pm 38)\%$  of the extrapolated level under the peak as the estimate for inelastic events in the intermediate geometry. In this geometry the highest inelastic contribution was for 9.9 GeV/c  $\pi^+$  at  $\theta_{c.m.} \sim 140^\circ$ , where  $\sim 30\%$  of the events under the  $\chi^2$  peak were estimated as inelastic. At 5.9 GeV/c this correction ranged from 1 to 5%. At 9.9 GeV/c and above, the typical inelastic contribution was  $\sim 15\%$ .

In the forward geometry it was possible to make an empirical determination of the shape of the inelastic contribution under the elastic peak. This was done by displacing the predicted proton track in such a way that true elastic events would be displaced from the  $\chi^2$  origin, but inelastic events would have the same distribution as previously. The  $\chi^2$  distribution after this was done was flat within statistics all the way down to zero. Hence, in the forward geometry the inelastic contribution was taken as the extrapolation of the flat  $\chi^2$  tail into the peak. The inelastic correction amounted at most to  $\sim 20\%$  of the events in the region of the  $\chi^2$  peak and was generally considerably lower.

#### H. Corrections and Errors

The measured cross sections were corrected for muons and electrons in the pion beam (2.5–4.5%); absorption

in counter telescopes, hydrogen target, and air (15–20%); decay of the scattered pions or kaons (1–15% for pions and  $\sim 15\%$  for kaons); background from empty target (0–10%); and scanning losses (2%). The inelastic background corrections have been discussed in Sec. II G.

Measurements showed that spark chamber and counter efficiencies were consistent with our assumed efficiency of 100%, except for chamber SC5 in the back geometry (see Sec. II E). Since SC5 was needed only to determine the percentage of inelastic events, an error in the estimate of the SC5 efficiency did not affect the elastic cross sections. The SC5 efficiency and the inelastic correction was determined separately for each back geometry entry in Table I. It turned out that SC5 was close to 100% efficient for those few experimental points where the inelastic background was significant.

The effective solid angles subtended by the defining trigger counters were determined using a Monte Carlo program which took into account target length, beam spot size, spread in beam angle and momentum, and multiple scattering. To first approximation the effective solid angles depended only on target length; hence, our result is essentially independent of any uncertainty in incoming beam or multiple scattering. We estimate the accuracy of the effective solid angle determination to be  $\pm 3\%$ .

Counting losses in the electronics were never greater than 1%, except when an anticounter was used in the beam itself downstream from the target; the counting loss correction then was as high as 9%.

Due to uncertainties in the preceding corrections, there is a combined uncertainty in the absolute normalization of the cross sections of  $\pm 5\%$ . Systematic errors which can vary from point to point have been combined in quadrature with the statistical errors and the combined error is listed in the final column of Table I.

### III. RESULTS

The complete results are given in Table I and displayed in Figs. 7–14. Note that the cross sections in Table I are the differential cross sections averaged over the bin widths specified in the second column of the table. In the case where the cross section is rapidly falling, or in the case of a dip in the angular distribution, the true cross section will be smaller than the average cross section given in the table. Enough information is contained in Table I for the reader to make his own shape-dependent corrections. In some of the high-momentum-transfer bins at high energies, no events were found. In such cases upper limits are given corresponding to what the result would have been had one event occurred in that bin.<sup>20</sup>

<sup>20</sup> If  $v_1$  is the value of an upper limit given in Table I, the reader may set his own confidence limit by using  $e^{-v/v_1}$  as the probability that the cross section be greater than  $v$ .

TABLE I. Elastic scattering cross sections are given in column 4 with powers of ten in parentheses.  $d\sigma/dt$  (or  $d\sigma/du$ ) is the differential cross section averaged over the interval of  $t$  (or  $u$ ) specified in the second column. The fifth column lists the 1-standard-deviation relative error between adjacent points of a given energy. In addition there is a  $\pm 5\%$  normalization error. Upper limits are given for those bins where no events were seen and are specified as the cross section corresponding to one event.

$-t$ (GeV/c) <sup>2</sup>	$\Delta t$ (bin width) (GeV/c) <sup>2</sup>	$\text{Cos}\theta$	$d\sigma/dt^a$ [mb/(GeV/c) <sup>2</sup> ]	Percent error	$-t$ (GeV/c) <sup>2</sup>	$\Delta t$ (bin width) (GeV/c) <sup>2</sup>	$\text{Cos}\theta$	$d\sigma/dt^a$ [mb/(GeV/c) <sup>2</sup> ]	Percent error
5.80 GeV/c $\bar{p}$ - $p$ (forward geom. I)					5.90 GeV/c $K^-$ - $p$ (forward geom. II)				
0.574	0.071	0.876	1.36(-1)	$\pm 17$	2.534	0.276	0.494	2.29(-3)	$\pm 56$
0.647	0.074	0.860	1.90(-1)	14	2.920	0.497	0.417	8.31(-4)	51
0.723	0.078	0.844	1.87(-1)	13	3.332	0.327	0.335	7.76(-4)	50
0.802	0.081	0.827	1.67(-1)	14	3.761	0.531	0.249	1.48(-4)	106
0.885	0.084	0.809	1.54(-1)	12	4.424	0.795	0.117	1.44(-4)	75
0.971	0.087	0.790	1.55(-1)	12	5.341	1.039	-0.066	<5.77(-5)	
1.059	0.090	0.771	9.47(-2)	13	9.71 GeV/c $K^-$ - $p$ (forward geom. I)				
1.150	0.092	0.752	7.33(-2)	13	0.760	0.138	0.911	1.27(-1)	28
1.244	0.095	0.731	6.84(-2)	12	0.904	0.149	0.895	5.04(-2)	17
1.340	0.097	0.711	3.19(-2)	17	1.058	0.159	0.877	3.99(-2)	16
1.488	0.200	0.679	2.27(-2)	14	1.222	0.169	0.857	1.86(-2)	19
1.691	0.206	0.635	1.45(-2)	17	1.395	0.177	0.837	1.29(-2)	23
1.900	0.212	0.590	8.89(-3)	21	1.576	0.186	0.816	7.21(-3)	29
2.114	0.216	0.544	8.67(-3)	22	1.866	0.393	0.782	3.01(-3)	25
2.331	0.218	0.497	8.79(-3)	24	2.271	0.418	0.735	1.04(-3)	36
2.550	0.220	0.449	4.70(-3)	36	3.039	1.118	0.645	8.60(-5)	71
2.826	0.331	0.390	4.99(-3)	38	4.181	1.167	0.512	<3.50(-5)	
5.90 GeV/c $\bar{p}$ - $p$ (forward geom. II)					5.457	1.385	0.363	<3.29(-5)	
2.590	0.339	0.452	4.22(-3)	28	13.57 GeV/c $K^-$ - $p$ (forward geom. I)				
2.929	0.340	0.380	5.16(-3)	22	1.208	0.242	0.901	1.45(-2)	38
3.324	0.449	0.297	1.35(-3)	28	1.460	0.262	0.880	1.14(-2)	37
3.768	0.440	0.202	4.60(-4)	53	1.879	0.577	0.846	1.09(-3)	71
4.201	0.425	0.111	<8.81(-5)		2.657	0.978	0.782	<2.92(-4)	
4.715	0.604	0.002	1.19(-4)	100	3.870	1.449	0.682	<1.84(-4)	
5.251	0.468	-0.111	2.30(-4)	58	5.80 GeV/c $\pi^-$ - $p$ (forward geom. I)				
5.743	0.516	-0.215	<1.18(-4)		0.572	0.070	0.886	4.92(-1)	15
9.71 GeV/c $\bar{p}$ - $p$ (forward geom. I)					0.644	0.074	0.872	2.71(-1)	11
0.761	0.139	0.908	9.35(-2)	30	0.720	0.077	0.857	1.94(-1)	7
0.905	0.150	0.891	4.98(-2)	21	0.799	0.080	0.841	1.50(-1)	10
1.060	0.160	0.872	2.82(-2)	24	0.880	0.083	0.825	1.15(-1)	8
1.313	0.348	0.841	5.91(-3)	40	0.965	0.086	0.808	8.22(-2)	10
1.678	0.381	0.797	2.53(-3)	48	1.053	0.089	0.791	7.64(-2)	8
2.073	0.409	0.749	1.32(-3)	49	1.143	0.091	0.773	6.29(-2)	8
2.493	0.432	0.699	1.09(-3)	50	1.235	0.093	0.754	5.82(-2)	9
3.048	0.679	0.632	5.85(-4)	50	1.329	0.095	0.735	4.44(-2)	7
4.096	1.416	0.505	<6.32(-5)		1.426	0.097	0.716	3.84(-2)	7
5.509	1.411	0.334	<7.07(-5)		1.524	0.099	0.697	2.70(-2)	8
5.80 GeV/c $K^-$ - $p$ (forward geom. I)					1.624	0.101	0.677	2.25(-2)	9
0.573	0.071	0.884	2.70(-1)	15	1.725	0.102	0.657	1.74(-2)	10
0.645	0.074	0.869	1.91(-1)	15	1.827	0.103	0.636	1.24(-2)	11
0.721	0.077	0.853	8.64(-2)	19	1.931	0.104	0.616	1.04(-2)	12
0.800	0.081	0.837	6.88(-2)	22	2.035	0.105	0.595	6.95(-3)	8
0.882	0.084	0.821	5.53(-2)	20	2.140	0.106	0.574	4.77(-3)	10
0.967	0.086	0.803	2.86(-2)	26	2.246	0.106	0.553	3.86(-3)	11
1.054	0.089	0.786	3.67(-2)	19	2.352	0.107	0.532	2.42(-3)	15
1.145	0.091	0.767	4.22(-2)	19	2.459	0.107	0.511	1.08(-3)	22
1.237	0.094	0.748	3.41(-2)	18	2.619	0.214	0.479	5.20(-4)	28
1.381	0.194	0.719	2.29(-2)	15	5.90 GeV/c $\pi^-$ - $p$ (forward geom. II)				
1.578	0.200	0.679	1.62(-2)	18	2.360	0.055	0.539	1.88(-3)	30
1.886	0.416	0.616	5.32(-3)	23	2.442	0.110	0.523	1.56(-3)	19
2.308	0.428	0.531	1.61(-3)	43	2.579	0.165	0.496	4.14(-4)	25
2.737	0.431	0.443	2.52(-3)	47	2.744	0.165	0.464	1.81(-4)	26

<sup>a</sup> Powers of ten in parentheses. The cross sections are averaged over the specified bin widths.



TABLE I (continued)

$-u$	$\Delta u$ (bin width)	$\text{Cos}\theta$	$d\sigma/du$	Percent error	$-u$	$\Delta u$ (bin width)	$\text{Cos}\theta$	$d\sigma/du$	Percent error
9.85 GeV/c $\pi^-p$ (back geom.)					9.85 GeV/c $\pi^+p$ (intermediate geom.)				
0.054	0.033	-0.990	1.69(-3)	$\pm 10$	2.288	0.520	-0.737	9.62(-6)	$\pm 82$
-0.003	0.027	-0.996	1.40(-3)	10	1.838	0.380	-0.788	3.74(-5)	42
-0.023	0.013	-0.998	1.66(-3)	10	1.517	0.262	-0.824	4.94(-5)	54
-0.034	0.008	-0.999	2.03(-3)	8	1.266	0.241	-0.852	1.28(-4)	26
13.73 GeV/c $\pi^-p$ (back geom.)					9.85 GeV/c $\pi^+p$ (back geom.)				
0.183	0.079	-0.983	3.02(-4)	24	0.180	0.051	-0.975	1.91(-4)	76
0.118	0.050	-0.988	4.59(-4)	20	0.132	0.045	-0.981	1.54(-4)	94
0.073	0.041	-0.992	5.03(-4)	23	0.054	0.033	-0.990	1.16(-3)	45
0.008	0.025	-0.997	8.82(-4)	15	-0.000	0.021	-0.996	3.96(-3)	21
-0.012	0.015	-0.999	1.01(-3)	15	-0.019	0.015	-0.998	7.28(-3)	11
-0.024	0.007	-0.9997	1.16(-3)	11	-0.032	0.011	-0.999	8.31(-3)	11
16.25 GeV/c $\pi^-p$ (back geom.)					13.73 GeV/c $\pi^+p$ (intermediate geom.)				
0.172	0.103	-0.987	3.56(-4)	29	2.824	0.691	-0.771	5.4 (-7)	290
0.089	0.063	-0.992	4.18(-4)	28	2.229	0.498	-0.819	2.1 (-6)	150
0.000	0.045	-0.998	4.15(-4)	79	1.810	0.340	-0.852	1.39(-5)	52
5.91 GeV/c $\pi^+p$ (intermediate geom.)					17.07 GeV/c $\pi^+p$ (back geom.)				
0.866	0.103	-0.819	2.24(-3)	15	0.012	0.027	-0.998	7.2 (-4)	90
0.766	0.098	-0.839	3.53(-3)	9	-0.009	0.016	-0.999	2.56(-3)	46
0.671	0.092	-0.857	3.92(-3)	10					
0.582	0.087	-0.875	5.60(-3)	8					
0.498	0.081	-0.891	5.48(-3)	8					
0.419	0.075	-0.906	5.34(-3)	7					
0.347	0.070	-0.920	4.21(-3)	8					
0.280	0.065	-0.933	2.56(-3)	10					
0.218	0.058	-0.945	1.87(-3)	13					
0.163	0.052	-0.956	1.28(-3)	17					
0.103	0.067	-0.968	1.17(-3)	29					
5.91 GeV/c $\pi^+p$ (back geom.)									
0.138	0.049	-0.961	5.52(-4)	71					
0.096	0.033	-0.969	2.68(-3)	23					
0.065	0.030	-0.975	4.98(-3)	16					
0.037	0.026	-0.981	8.51(-3)	13					
0.013	0.023	-0.986	1.35(-2)	10					
-0.026	0.016	-0.993	2.21(-2)	8					
-0.041	0.015	-0.996	3.09(-2)	5					
-0.053	0.008	-0.998	3.62(-2)	5					
-0.059	0.005	-0.999	3.76(-2)	4					

TABLE II. Exponential fit of backward peaks. The quantities  $A$  and  $B$  are the least-squares fits to the form  $d\sigma/du = Ae^{Bu}$ . The regions used in the fit are  $|u| < 0.8$  (GeV/c)<sup>2</sup> for  $\pi^-p$  and  $|u| < 0.1$  (GeV/c)<sup>2</sup> for  $\pi^+p$ .

Incident momentum (GeV/c)	Pion charge	$A$ [ $\mu\text{b}/(\text{GeV}/c)^2$ ]	$B$ [ $(\text{GeV}/c)^{-2}$ ]
5.9	+	15.1 $\pm$ 0.4	16.1 $\pm$ 0.5
9.9	+	4.27 $\pm$ 0.30	22.9 $\pm$ 2.7
13.9	+	2.69 $\pm$ 0.74	24.7 $\pm$ 8.0
17.1	+	2.4 $\pm$ 1.1	
5.9	-	4.94 $\pm$ 0.12	3.72 $\pm$ 0.08
9.9	-	1.70 $\pm$ 0.06	4.05 $\pm$ 0.16
13.7	-	0.95 $\pm$ 0.07	6.62 $\pm$ 0.94
16.25	-	0.45 $\pm$ 0.11	

### A. $\pi^-p$ Backward Peaks

The data for  $\pi^-p$  scattering from the back and intermediate geometries are shown in Fig. 7. In the region  $|u| < 0.8$  (GeV/c)<sup>2</sup> the peak fits a simple exponential  $d\sigma/du = Ae^{Bu}$  with a slope  $B \approx 4$  (GeV/c)<sup>-2</sup>; thus, the  $\pi^-p$  backward peak is about twice as wide as most forward peaks. Least-squares fits of the above form to the data for  $|u| < 0.8$  (GeV/c)<sup>2</sup>, shown as straight lines, give solutions for  $A$  and  $B$  shown in Table II. Note that  $A$  (which is the  $u=0$  cross section) is decreasing with increasing energy and is consistent with the power law  $d\sigma/dw|_{u=0} \propto s^{2\alpha-1}$ , where  $\alpha = -0.05 \pm 0.04$ . The slope  $B$  is increasing with increasing energy. Our observed rate

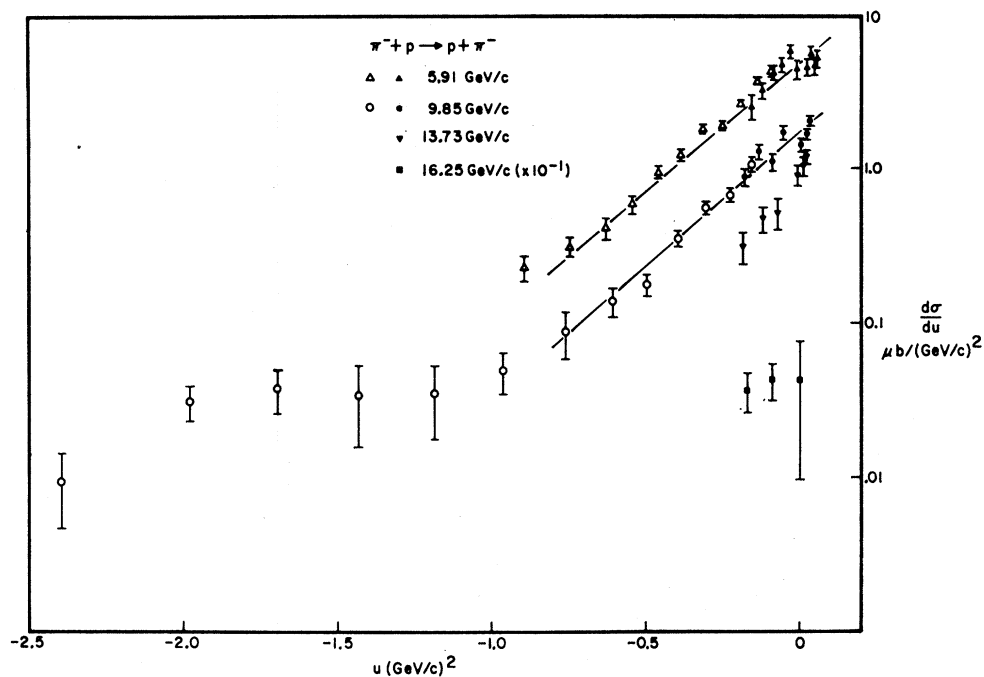


FIG. 7. Angular distributions of the backward  $\pi^-p$  elastic scattering. The open symbols are from the intermediate geometry and the solid symbols are from the back geometry. " $\mu^2$ " is the square of the crossed four-momentum transfer. The straight lines represent the least-squares fits described in the text. The 16.3-GeV/c results are plotted one decade lower.

of shrinkage is in quantitative agreement with the simplest type of Regge-pole parametrization.<sup>4</sup> At 5.9 GeV/c the least-squares fit corresponds to a  $\chi^2$  proba-

bility of 0.3%, which suggests that the true shape may depart from the straight line. It appears that there may be a flattening of the backward peak near 180°. At 9.9

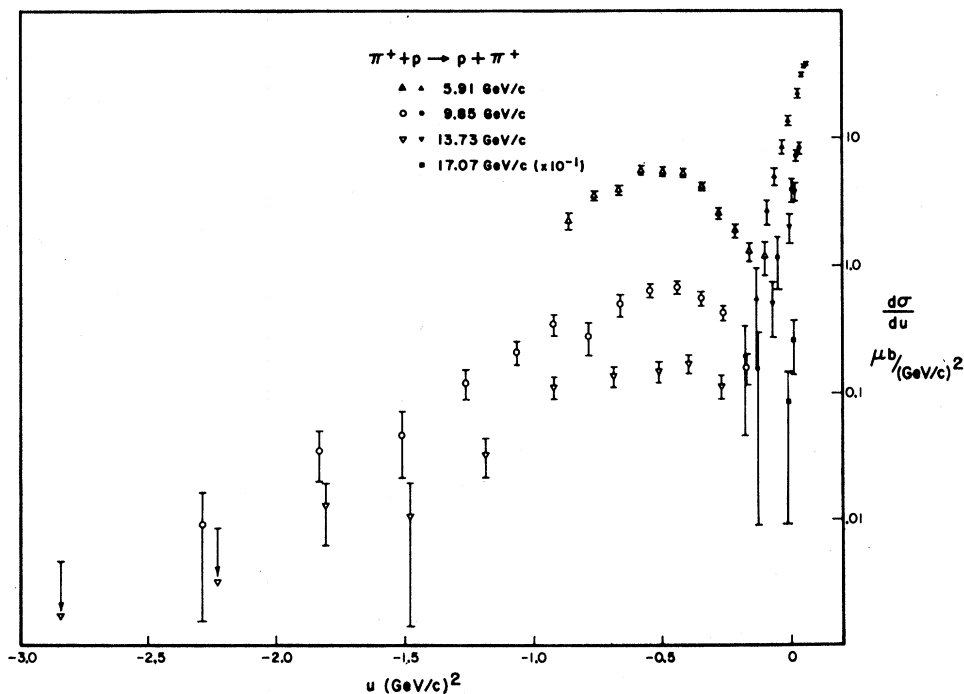


FIG. 8. Angular distribution of the backward  $\pi^+p$  elastic scattering. The open symbols are from the intermediate geometry. The three "points" which represent upper limits are set at 2 standard deviations. The 17.1-GeV/c results are plotted one decade lower.

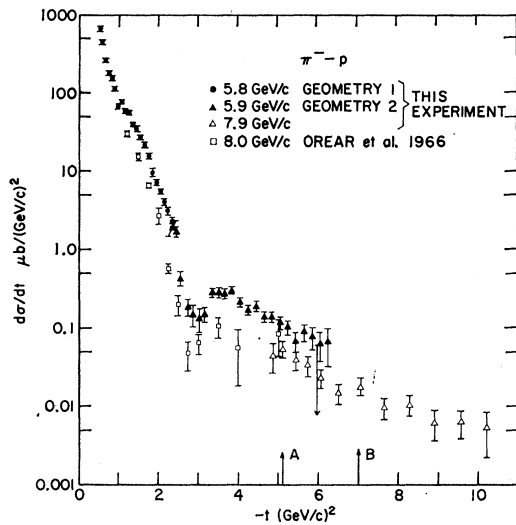


FIG. 9. Angular distributions for  $\pi^-p$  elastic scattering. The data at small  $|t|$  for 8.0 GeV/c are from Ref. 1. The arrows on the abscissa marked A and B indicate  $90^\circ$  (c.m. system) for 5.9 and 7.9 GeV/c, respectively.

GeV/c, the  $\chi^2$  probability for the straight-line fit is 7%. The cross section appears to be approximately constant in the region  $-2 < u < -1$  (GeV/c) $^2$  but in the region  $u \sim -3$  (GeV/c) $^2$  the cross section drops another factor of  $\sim 30$ . Our results are not quite consistent with those at 8 and 16 GeV/c from the BNL-Carnegie-Mellon

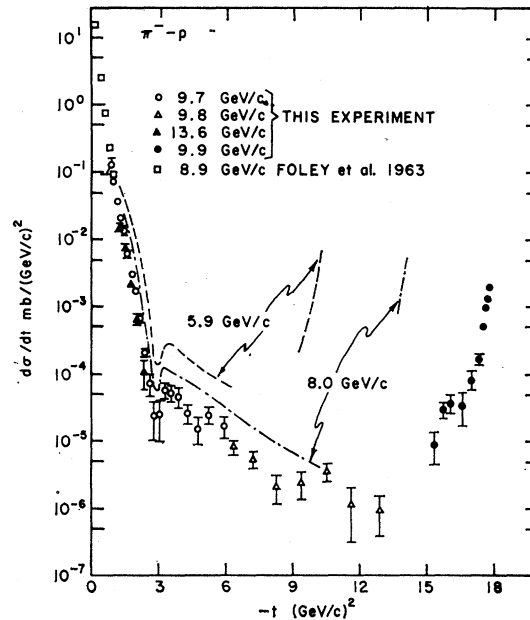


FIG. 10. The complete angular distribution for  $\pi^-p$  elastic scattering at approximately 10 GeV/c. Representative points at small  $|t|$  are taken from the 8.9-GeV/c data of Ref. 5. The dashed lines approximate the data from Figs. 7 and 9 and Ref. 21.

group, but are in good agreement with 6.9-GeV/c preliminary results from CERN.<sup>21</sup>

The data from the back and intermediate geometries

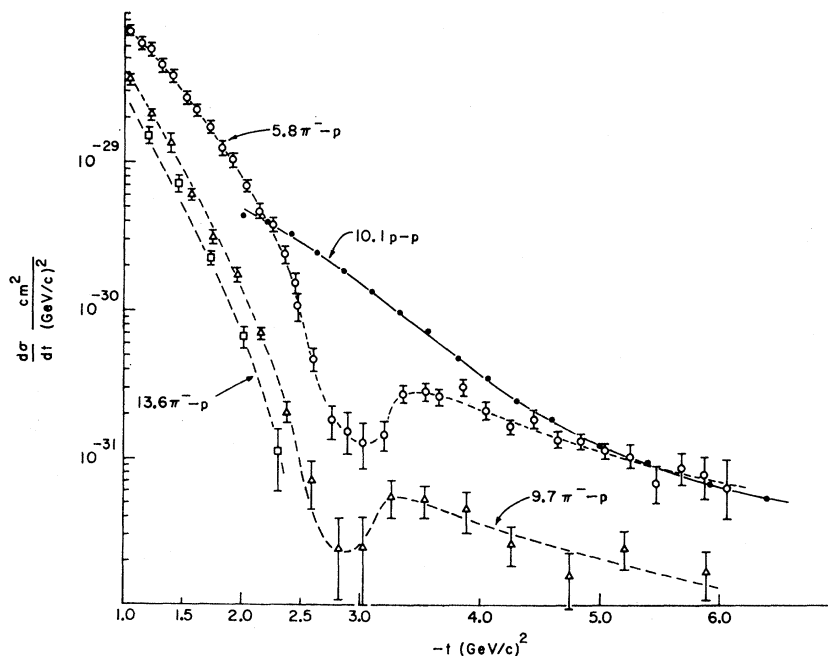


FIG. 11. Enlarged view of the region  $1 < -t < 6$  (GeV/c) $^2$  for  $\pi^-p$  elastic scattering. The smooth curves are drawn by hand. In drawing the curve for 13.6 GeV/c the correction for finite bin width described in the text was made; hence, this line lies about 8% below the data points of Table I. For comparison the 10.1 GeV/c  $p-p$  results of Ref. 28 are also shown.

<sup>21</sup> E. W. Anderson, E. J. Bleser, H. R. Blieden, G. B. Collins, D. Garelick, J. Menes, F. Turkot, D. Birnbaum, R. M. Edelstein, N. C. Hien, T. J. McMahon, J. Mucci, and J. Russ, Phys. Rev. Letters **20**, 1529 (1968); W. F. Baker, K. Berkelman, P. J. Carlson, G. P. Fisher, P. Fleury, D. Hartill, R. Kalbach, A. Lundby, S. Mukhin, R. Nierhaus, K. P. Pretzl, and J. Wouds, Phys. Letters **28B**, 291 (1968).

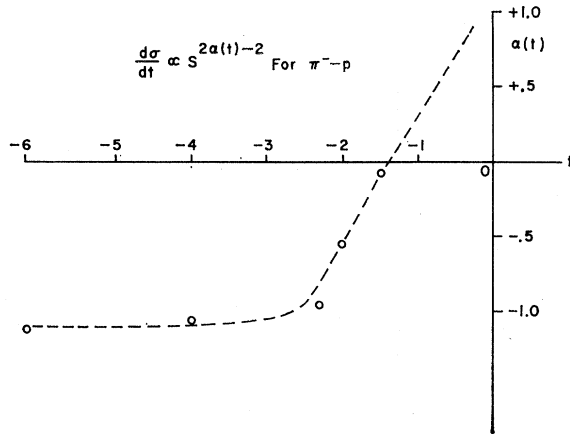


FIG. 12. Plot of  $\alpha$  versus  $t$  assuming a power-law energy dependence  $d\sigma/dt \propto s^{2\alpha-2}$  for the curves of Fig. 11.

for  $\pi^+p$  scattering are shown in Fig. 8. Here again is a backward peak rising at least three orders of magnitude but with a sharp dip superimposed. The location of the dip appears to be independent of  $u$ , and our estimate of the position of its minimum is  $u = -0.13 \pm 0.05$   $(\text{GeV}/c)^2$ . The cross section in the dip is about an order of magnitude lower than a smooth continuation of the remainder of the curve, and the full width at half "depth" appears to be  $\sim 0.1$   $(\text{GeV}/c)^2$ . Since the bin widths of the data points in the region of the dip are  $\sim 0.05$   $(\text{GeV}/c)^2$ , the corrections for experimental resolution may be important. We estimate that the true cross sections at the bottom of the dip are  $0.75 \pm 0.25$  and  $0.1 \pm 0.05$   $\mu\text{b}/(\text{GeV}/c)^2$  at 5.9 and 9.9  $\text{GeV}/c$ , respectively. This would make the  $\pi^+p$  cross section at the center of the dip perhaps an order of magnitude smaller than the corresponding  $\pi^-p$  cross section, in contrast to values at  $180^\circ$ , where the  $\pi^+p$  cross section is about five times larger than the  $\pi^-p$  cross section.

Although it is probably incorrect to fit the  $\pi^+p$  cross sections near  $180^\circ$  with straight lines since the slope is not constant, average slopes obtained by fitting the data in the region  $|u| < 0.1$   $(\text{GeV}/c)^2$  are given in Table II; they range 16–25  $(\text{GeV}/c)^{-2}$ .

All the features of both the  $\pi^-$  and  $\pi^+$  backward peaks for  $|u| < 1$   $(\text{GeV}/c)^2$  have been fit surprisingly well by a simple Reggeized baryon exchange model.<sup>4</sup> Reggeized baryon exchange predicts the dip in the  $\pi^+p$  backward peak since the nucleon exchange trajectory goes through a nonsense value of the wrong signature at  $u \approx -0.15$   $(\text{GeV}/c)^2$ .<sup>22</sup> In  $\pi^-p$  scattering, the nucleon exchange cannot contribute because a doubly charged baryon is needed for the exchange, and the prediction is for no dip. Using only straight-line Regge trajectories and essentially constants for residue functions, a least-

<sup>22</sup> C. B. Chiu and J. D. Stack, Phys. Rev. **153**, 1575 (1967).

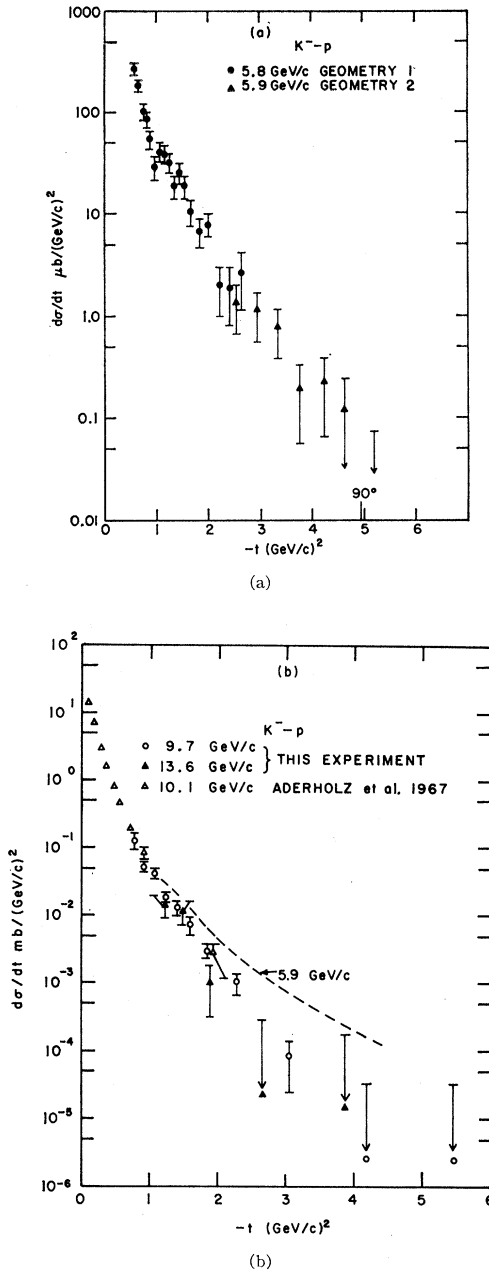


FIG. 13. Angular distributions for  $K^-p$  elastic scattering at 5.8, 9.7, and 13.6  $\text{GeV}/c$ . When no events were observed in a bin, an upper limit is shown, corresponding to one event. The 5.9- $\text{GeV}/c$  results are shown in (a) and the 9.7- and 13.6- $\text{GeV}/c$  results are shown in (b), which also has plotted data points from Ref. 31.

squares fit to our data<sup>4</sup> gives

$$\alpha_N(u) = -0.38 + 0.88u,$$

$$\alpha_\Delta(u) = 0.19 + 0.87u.$$

This is to be compared with the usual Chew-Frautschi trajectories determined from the nucleon and isobar

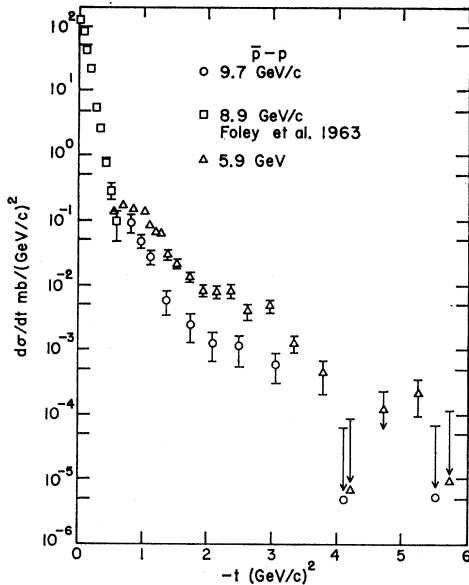


FIG. 14. Angular distributions for  $\bar{p}$ - $p$  elastic scattering at 5.9 and 9.7 GeV/ $c$ . Some 8.9-GeV/ $c$  points at small  $|t|$  from Ref. 5 are shown.

masses:

$$\alpha_N(u) = -0.39 + 1.0u,$$

$$\alpha_\Delta(u) = 0.15 + 0.9u.$$

The agreement is obviously good.

## B. Forward Geometry Results

### 1. $\pi^-$ - $p$

In Fig. 9,  $\pi^-$ - $p$  angular distributions are shown for 5.9 and 7.9 GeV/ $c$ ; data points are from this experiment and Ref. 1. Figure 10 shows data at 9.9 and 13.6 GeV/ $c$  together with freehand curves through the points of Fig. 9; also shown are data from Fig. 7 and from Ref. 5. The shapes of the angular distributions are similar at all energies, showing a cross section which decreases rapidly from  $t=0$  to  $t \approx -2.5$  (GeV/ $c$ ) $^2$ , a slower fall at wider angles, and then a strong backward peak near 180°. At 9.9 GeV/ $c$  the cross section decreases by more than seven decades in going from 0° to 120° c.m. system, and then the backward peak rises by a factor of 2000. At all momenta above 3 GeV/ $c$  structures in the  $\pi^-$ - $p$  angular distribution appear at  $-t \approx 1$  and 3 (GeV/ $c$ ) $^2$ . At momenta below 4 GeV/ $c$ , the structure at  $-t \approx 1$  (GeV/ $c$ ) $^2$  is an appreciable dip,<sup>23,24</sup> but this becomes less marked with increasing momentum. However, in our 13.6 GeV/ $c$  data there is still a change in slope of the angular distribution at this  $t$  value, and similar behavior is present in  $\pi^+$ - $p$  scattering.<sup>1</sup> Our

<sup>23</sup> C. T. Coffin, N. Dikman, L. Ettlinger, D. Meyer, A. Saulys, K. Terwilliger, and D. Williams, Phys. Rev. **159**, 1169 (1967).

<sup>24</sup> M. L. Perl, Y. Y. Lee, and E. Marquit, Phys. Rev. **138**, 707 (1965).

5.9-, 7.9-, and 9.9-GeV/ $c$  results show a sharp dip at  $-t \approx 3$  (GeV/ $c$ ) $^2$ , but it is not possible to say whether this dip is also becoming less pronounced with increasing momentum. It has been pointed out<sup>25</sup> that this effect may be a continuation of a dip which appears in lower-energy  $\pi^-$ - $p$  scattering.<sup>26,27</sup> At momenta above 4 GeV/ $c$  no accurate measurements of  $\pi^+$ - $p$  scattering exist in the region  $-t \approx 3$  (GeV/ $c$ ) $^2$ , so it is not known whether the  $\pi^+$ - $p$  angular distribution has a similar dip. The region of this dip is shown in expanded scale in Fig. 11, with  $p$ - $p$  data shown for comparison.<sup>28</sup> The smooth curves in Fig. 11 are consistent with a Regge-type power-law dependence  $d\sigma/dt \propto s^{2\alpha(t)-2}$ , and in Fig. 12 we show  $\alpha(t)$  derived in this way. For  $|t| > 3$  (GeV/ $c$ ) $^2$  we find  $\alpha(t) \approx -1$ , but in the region  $-3 < t < -1$  (GeV/ $c$ ) $^2$ ,  $\alpha(t)$  is increasing linearly with  $t$  and would extrapolate to  $\alpha(0) = +1$  with the "usual" Regge trajectory slope of 0.8 GeV $^{-2}$ . Although such behavior is consistent with the earliest ideas of vacuum trajectory contribution,<sup>29</sup> current interpretations invoke other Regge trajectories.<sup>25,30</sup> We have no evidence that the higher-energy cross sections are reaching an asymptotic limit at fixed  $t$ .

The forward peak in the region  $|t| < 1$  (GeV/ $c$ ) $^2$  fits the simple exponential  $e^{Bt}$  quite well, with  $B \approx 8$  (GeV/ $c$ ) $^{-2}$  independent of the pion energy.<sup>5</sup> It is interesting that for  $|t| < 1$  (GeV/ $c$ ) $^2$  one does not observe the shrinkage predicted by the simplest Regge interpretation,<sup>29</sup> whereas for  $|t| > 1$  (GeV/ $c$ ) $^2$  one does observe considerable shrinkage.

### 2. $K^-$ - $p$

The results for  $K^-$ - $p$  elastic scattering are shown in Fig. 13 together with some smaller-angle data.<sup>31</sup> The only structure evident within our statistics is a change of slope of the differential cross section at  $-t \approx 1$  (GeV/ $c$ ) $^2$ . With 2–4 GeV/ $c$  incident kaons, there is a dip in the angular distribution at  $-t \approx 1$  (GeV/ $c$ ) $^2$ ,<sup>32</sup> and as in the  $\pi^-$ - $p$  case, we have a dip at this  $t$  value which

<sup>25</sup> N. E. Booth, Phys. Rev. Letters **21**, 465 (1968).

<sup>26</sup> S. W. Kormanyos, A. D. Krisch, J. R. O'Fallon, L. G. Ratner, and K. Ruddick, Phys. Rev. Letters **16**, 709 (1966).

<sup>27</sup> A. S. Carroll, J. Fischer, A. Lundby, R. H. Phillips, C. L. Wang, F. Lobkowicz, A. C. Melissinos, Y. Nagashima, and S. Tewksbury, Phys. Rev. Letters **20**, 607 (1968).

<sup>28</sup> J. V. Allaby, F. Binon, A. N. Diddens, P. Duteil, A. Klovning, R. Meunier, J. P. Peigneux, E. J. Sacharidis, K. Schlipmann, M. Spighel, J. P. Stroot, A. M. Thorndike, and A. M. Wetherell, Phys. Letters **28B**, 67 (1968). Reference to earlier CERN experiments are given here.

<sup>29</sup> S. C. Frautschi, M. Gell-Mann, and F. Zachariasen, Phys. Rev. **126**, 2204 (1962).

<sup>30</sup> V. Barger and R. J. N. Phillips, Phys. Rev. Letters **20**, 564 (1968).

<sup>31</sup> M. Aderholz *et al.* [Aachen-Berlin-CERN-London (I.C.)-Vienna Collaboration], Phys. Letters **24B**, 434 (1967).

<sup>32</sup> R. Crittenden, H. Martin, W. Kernan, L. Leipuner, A. Li, F. Ayer, L. Marshall, and M. Stevenson, Phys. Rev. Letters **12**, 429 (1964); M. Dickinson, S. Miyashita, L. Marshall Libby, and P. Kearney, Phys. Letters **24B**, 596 (1967); M. Focacci, S. Focardi, G. Giacomelli, P. Serra, M. Zerbetto, and L. Monari, *ibid.* **19**, 441 (1965); J. Gordon, *ibid.* **21**, 117 (1966).

becomes less prominent with increasing momentum. For  $|t| < 0.75$  (GeV/c)<sup>2</sup>, it is known that the  $K^-p$  scattering fits a simple exponential with little shrinkage.<sup>5</sup> For  $|t| > 1$  (GeV/c)<sup>2</sup>, there is a definite decrease of  $d\sigma/dt$  at fixed  $t$  with increasing energy; however, the rate of decrease is considerably smaller for  $K^-p$  than for  $\pi^-p$ .

### 3. $\bar{p}p$

Results for  $\bar{p}p$  elastic scattering are shown in Fig. 14, together with some smaller-angle data.<sup>5</sup> At lower momenta, there is a dip in the cross section at  $-t \approx 0.5$  (GeV/c)<sup>2</sup><sup>33</sup> followed by a hump which is still present in our results at 5.9 GeV/c, and to a lesser extent at 9.7 GeV/c. We also see a similar structure, or "shoulder," in the region  $2 < -t < 3$  (GeV/c)<sup>2</sup>. The two "dips" at  $-t \approx 0.5$  and  $1.8$  (GeV/c)<sup>2</sup> are suggestive of minima followed by secondary maxima of a black-disk diffraction pattern. As in the  $\pi^-p$ , there is considerable decrease in cross section with increasing momentum at large momentum transfers, whereas for  $|t| < 0.5$  (GeV/c)<sup>2</sup> in the  $\bar{p}p$  case, the cross sections actually increase with increasing momentum.<sup>5</sup>

### 4. Comparison of Large-Angle Scattering of Different Particles on Protons

For values of  $|t| > 1$  (GeV/c)<sup>2</sup>,  $\pi^-$ ,  $K^-$ , and  $\bar{p}$  scattering on protons at the momenta studied here all have approximately the same order of magnitude, while all falling several decades. The magnitude, however, is considerably lower than cross sections for  $p-p$ <sup>28,34</sup> or  $n-p$ <sup>35</sup> scattering (see Fig. 11). Agreement between  $\pi^-p$  and  $p-p$  at least is considerably improved if the reactions are compared at the same c.m. kinetic energy.

Angular distributions for  $\pi^-p$ ,  $\bar{p}p$ , and probably to a lesser extent  $K^-p$  have considerable structure for

incident momenta at least as high as 10 GeV/c; for  $p-p$  scattering such structure is very much smaller.<sup>28</sup> The values of momentum transfer at which the structures are observed appear to be independent of incident momentum. There seems to be three different kinds of dips: (1) those which decrease with increasing energy [the dips at  $-t \sim 1$  (GeV/c)<sup>2</sup> in  $\pi^-p$ ,  $K^-p$ , and  $\bar{p}p$ ], (2) those which increase with increasing energy [the  $p-p$  dip at  $-t \sim 1$  (GeV/c)<sup>2</sup> and possibly the backward  $\pi^+p$  dip], and (3) those which stay about the same [the  $-t \sim 3$  (GeV/c)<sup>2</sup> dip in  $\pi^-p$ ]. In all these reactions  $d\sigma/dt$  at fixed  $t$  decreases with increasing energy in the region  $-t > 1$  (GeV/c)<sup>2</sup>; however, the amount of decrease varies considerably with the reaction. Explanations have been given for some of the structures observed here. Regge models<sup>30</sup> can give dips in the cross sections where exchange amplitudes pass through zero in a manner analogous to the dip in  $\pi^+p$  backward scattering. Quark models which include multiple scattering contributions give dips,<sup>36</sup> as can an optical model theory which takes into account the finite extensions of both of the interacting particles.<sup>37</sup> It is not possible at present to decide between the various theories.

### ACKNOWLEDGMENTS

An experiment such as that described here requires the efforts of a great many people other than those given as authors of the publication, and we are obviously indebted to many persons for the success of this work. A very abbreviated list of people to whom we owe special thanks follows: Dr. R. Cool, for his advice and encouragement; the AGS staff, in particular, Dr. J. Sanford, T. Blair, and J. Lypecky, for their cooperation and support; Dr. T. Kycia, for the loan of his differential Čerenkov counters; the technical support of G. Munoz, T. Reitz, H. Sauter, F. Seier and O. Thomas; and the film scanners at Cornell and Brookhaven for their excellent work.

<sup>33</sup> W. M. Katz, B. Forman, and T. Ferbel, Phys. Rev. Letters **19**, 265 (1967).

<sup>34</sup> C. M. Ankenbrandt, A. R. Clark, B. Cork, L. T. Kerth, and W. A. Wenzel, Phys. Rev. **170**, 1223 (1968).

<sup>35</sup> M. N. Kreisler, F. Martin, M. L. Perl, M. J. Longo, and S. T. Powell, Phys. Rev. Letters **16**, 1217 (1966).

<sup>36</sup> D. R. Harrington and A. Pagnamenta, Phys. Rev. Letters **18**, 1147 (1967); Phys. Rev. **173**, 1599 (1968).

<sup>37</sup> T. T. Chou and C. N. Yang, Phys. Rev. Letters **20**, 1213 (1968).